Journal of
Laser Applications

ARTICLE

scitation.org/journal/jla

Fusing optical coherence tomography and photodiodes for diagnosis of weld features during remote laser welding of copper-to-aluminum

Cite as: J. Laser Appl. **35**, 012018 (2023); doi: 10.2351/7.0000803
Submitted: 27 June 2022 · Accepted: 20 December 2022 ·
Published Online: 17 January 2023

View Online Export Citation CrossMark

Tine Brežan,[1] Pasquale Franciosa,[2] Matija Jezeršek,[1] and Dariusz Ceglarek[2]

AFFILIATIONS

[1] Faculty of Mechanical Engineering, University of Ljubljana, Ljubljana, Slovenia
[2] WMG, The University of Warwick, Coventry CV4 7AL, United Kingdom

Note: Paper published as part of the special topic on Proceedings of the International Congress of Applications of Lasers & Electro-Optics 2022.

ABSTRACT

This study has been designed to investigate whether variations in the features of laser weldments can be isolated and diagnosed by fusing photodiodes and optical coherence tomography (OCT). Two manufacturing scenarios (variation in laser power and focal offset) have been considered during remote laser welding of 0.2 mm thick Cu foils on 2 mm thick Al 1050 plates with an adjustable ring mode laser integrated with a 1D oscillation head. The process was monitored by measuring weld penetration depth with OCT and by process emissions (plasma and back-reflection) via photodiodes. The acquisition frequency of all signals was 40 kHz. Strong correlations ($r > 0.75$) were shown between plasma, back-reflection, and OCT signals and measured depth and width of the weld. Weak correlations ($r < 0.5$) between voids, cracks, and sensor signals were observed. Although plasma is the predominant signal that carries most of the information about the process, and the OCT allows direct measurement of the penetration depth, their integration reached 87% classification accuracy of the tested welding scenarios. The main misclassification was observed between "good weld" and "over weld," defined by the measured weld depth. Sensor fusion strategies with manufacturing implications are discussed throughout the paper.

Key words: remote laser welding, copper-to-aluminum welding, optical coherence tomography, photodiodes, sensor fusion

© *2023 Author(s). All article content, except where otherwise noted, is licensed under a Creative Commons Attribution (CC BY) license (http://creativecommons.org/licenses/by/4.0/).* https://doi.org/10.2351/7.0000803

I. INTRODUCTION

E-mobility presents a path to the future of global transportation. Owing to stricter regulations involving CO_2 emissions, automotive manufacturers are increasingly investing in electric vehicles (EVs). Joining of dissimilar metal components, such as Cu/Al, leads the way to build electric subsystems such as battery modules, cell connectors/tabs, and power electronics. Due to strict performance requirements of EV components, where a single defective weld can present a malfunction of the entire system, and the need to produce EVs at a mass-scale in order to meet policy targets, the demand for zero-defect manufacturing has risen significantly.

Remote laser welding (RLW) is the process of choice for a wide range of applications in EV manufacturing and consists of a high-power laser source, scanning optics, and a robot manipulator. Due to the flexibility and high processing speed of guiding the laser beam over complex-shaped weld pieces, the technology has brought great attention.[1] Fortunato *et al.*[2] studied combinations of Cu-to-Al and Al-to-Cu in partial overlap laser welding with a wobbling scanning strategy; they reported deeper penetrations in Al-to-Cu welding and an overall better process window for Al on top, while Cu on top presented difficulties to fine-tune and control the penetration depth. Due to the low absorptivity of copper at ambient temperature and the difference in thermal properties of Cu/Al, the control of the welding process remains a major challenge.

In this regard, sensor technologies for inprocess monitoring of laser weldments have attracted significant interest. Recent results show that monitoring and control of the laser power during the adaptive 3D beam positioning can achieve a stable welding process and improved weld quality.[3–5] Chianese *et al.*[6] investigated the use of photodiodes for the detection of variations in the part-to-part gap and weld penetration depth during RLW of Cu-to-steel for battery tab connectors. Findings showed a strong correlation between the plasma signal and both part-to-part gap and weld penetration depth.

While photodiodes are widely used sensors due to their simple structure and low cost,[7] they only provide indirect measurements in the form of correlated signals (plasma, temperature, and back-reflection) to the actual weld features (i.e., weld penetration depth, etc.). Additionally, determining the correlation demands lengthy metallographic analyses, which incur significant cost and manual labor.[8] Conversely, optical coherence tomography (OCT) has shown promising results toward direct measurement of the weld penetration depth. Recent advances have shown the possibility to use OCT for preprocess, inprocess, and postprocess monitoring and control by its insusceptibility to other optical distortions.[9–12] Sokolov *et al.*[13] researched OCT sensors for RLW to enable a closed-loop control for the gap-to-gap bridging of aluminum plates. Their work confirmed the use of the OCT sensor to control and measure weld penetration depth. In Ref. 14, researchers demonstrated the use of the OCT sensor for welding thin Al–Cu foils used in automotive tab connectors and presented the use of TwinTec technology in conjunction with the OCT sensor. They proved an improvement in the stability of the molten pool by using an adjustable ring mode (ARM) laser. However, the study concluded that the accuracy was highly sensitive to the selection of the welding process parameters. Therefore, the sensor needed to be re-calibrated every time any process parameter was about to be changed. Furthermore, the absence of the keyhole mode would have made the OCT sensor unsuitable for measuring the weld penetration depth.

Although both OCT and photodiodes have been individually researched, the fusion of both sensors remains an under-explored area of investigation, especially for thin foils (below 0.5 mm) applications. This paper has been designed to explore opportunities for the inprocess monitoring and classification of weld features, based on the fusion of OCT and photodiode sensors, for variations of laser power and focal offset. The methodology is demonstrated on the RLW of the Cu foil (0.2 mm) in lap weld to Al plate using 1D beam oscillation and ARM laser. The selected materials are highly relevant for manufacturing EV components, such as battery cells and busbars.

II. MATERIALS AND METHODS

A. Experimental setup

The RLW experimental system, shown in Fig. 1 consisted of the multimode coherent fiber laser HighLight FL-ARM 10 000 coupled with the WeldMaster Scan&Track remote welding head (YW52 Precitec GmbH, Germany). Detailed parameters are in Table I. Experiments were conducted in an overlap configuration of 0.2 mm thick Cu foil (uncoated) on top of 2 mm thick Al plates (Al alloy grade 1050). Dimensions of specimens were 38 × 120 mm. The specimens were positioned on the working table by four individual clamps to assure zero gap between Cu and Al plates.

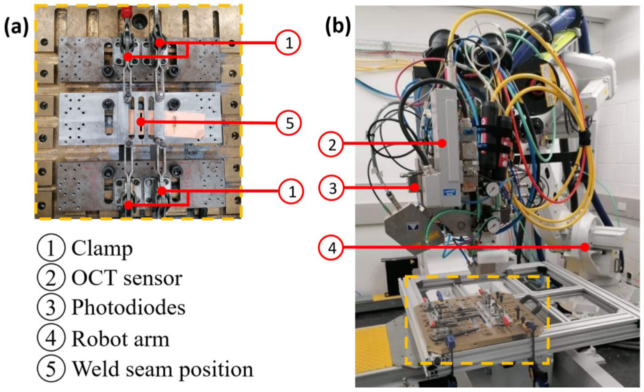

FIG. 1. (a) Clamping setup, (b) welding setup with a robot arm and tested sensors.

The laser welding process was monitored by an OCT sensor and two photodiodes (Precitec, GmbH, Germany), which were installed co-axially below the collimator of the welding head. Signals from all three sensors were synchronously sampled with a frequency of 40 kHz.

Figure 2 shows the conceptual optical arrangement: the first photodiode detects plasma radiation (P) in the spectral range 300–700 nm, while the second photodiode (R) detects laser back-reflection within the spectral range 1020–1090 nm. The system also consisted of a third photodiode (T), sensitive in the IR spectrum (900–1600 nm), though it was not used due to evidence indicating a strong correlation to the plasma signal.[6] Both OCT and photodiodes were manually aligned to the center of the molten pool/keyhole. OCT beam position was pre-optimized during a preliminary screening session, and the alignment was kept the same during all experiments. The photodiodes were also calibrated in such a way that both hardware and software gains were set to clamp the signals in the range [0, 10] V.

B. Process parameters and design of experiments

To evaluate the synergy between photodiodes and OCT and the use in an industrial environment, two groups of experiments

TABLE I. Laser welding system specifications.

Parameters	Units	Core	Ring
Max power	W	5000	5000
Optical fiber diameter	μm	100	290
Spot diameter on focus	mm	0.2	0.58
Rayleigh length	mm	2.6	6.2
Collimating length	mm	150	
Focusing length	mm	300	
Wavelength	nm	1070 ± 10	

© Author(s) 2023

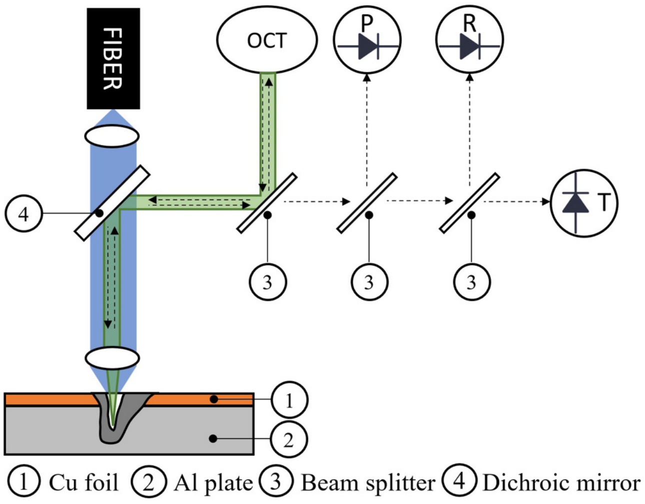

FIG. 2. Optical arrangement of OCT and photodiodes.

were conducted by choosing three different laser core powers (P_C) and four different values of the focal offset (A_Z) as shown in Table II. For each set of parameters, three repetitions were conducted (and four repetitions for $P_C = 1400$ W and $A_Z = 5$ mm). Other welding parameters were constant for both groups: the laser beam motion was composed of linear oscillation with frequency $f = 400$ Hz and amplitude $A_Y = 0.2$ mm with motion speed $S_X = 180$ mm/s. Ring power (P_R) was 3500 W.

Process parameters were determined during preliminary tests, with the aim of achieving a stable welding process. The process was started at $P_R = 1000$ W, $P_C = 1000$ W, $S_X = 50$ mm/s, and without beam oscillation. Several trials were performed, where laser parameters were systematically varied, and beam oscillation was added. At low welding speeds (<80 mm/s), transitions from no penetration of the copper foil to full burn-through were observed. The main reasons for this instability are related to the high thickness ratio between Cu foil and Al (1:10) and the temperature dependence of Cu's absorption coefficient (in the IR spectral region) and other thermal characteristics.

Since the thickness ratio is application-driven, we can only tackle the challenge related to the thermal dependence of the absorption coefficient. Once the keyhole is achieved, the absorption significantly increases and, consequently, the problem of process stability is minimized. Researchers have used different techniques such as wobbling of laser beam,[15] shaping of the laser beam profile, such as ARM technique,[14] and high welding speed to stabilize the welding process.[16] Miyagi *et al.*[16] also showed that welding speeds above 167 mm/s can suppress the occurrence of spatters and voids. Therefore, this paper implements the ARM laser with lateral oscillation (perpendicular to the weld seam direction) at a welding speed of 180 mm/s. With this speed, a wider process window and greater weld stability were achieved.

TABLE II. Definition of tested welding groups.

Process parameters	Variation of core power (group [1])	Variation of focal offset (group [2])
P_C (W)	700/1400/2300	1400
A_Z (mm)	5	3/5/7/10

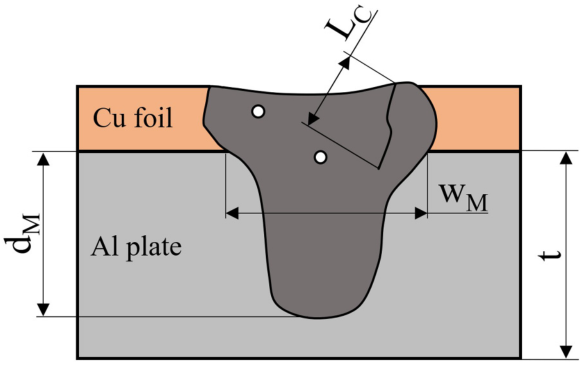

FIG. 3. Definition of weld features ("t" denotes the thickness of the Al plate).

The length of the welds was 30 mm. All experiments were conducted without inert gas and a filler wire.

In the first group of experiments (*group* [1]), the power of the core beam was varied to emulate manufacturing scenarios with variable weld penetration depth and, eventually, variations of absorptivity. Tests were carried out for $P_C = 700$, 1400, and 2300 W.

In the second group of experiments (*group* [2]), the effect of focal offset was studied. A focal offset can originate from nonrepeatable clamping, inaccurate robot motion, or thermal lensing. The focal offset, relative to the top surface of the Cu plate, was $A_Z = 3$, 5, 7, 10 mm. Corresponding beam spot diameters (for the core beam) were Ø0.31, Ø0.43, Ø0.57, and Ø0.79 mm, respectively.

Pictures of the front and back sides of the welded specimens were acquired with a digital camera (Nikon D3100). Each specimen was cut at two cross sections (at 10 and 20 mm from the start of the weld), which were then grinded and polished. Pictures of the cross sections were taken using an optical microscope (Leica stereo microscope M60). Weld width (w_M) and weld depth (d_M) were measured from the images as schematically shown in Fig. 3. Both dimensions were measured according to the Cu–Al interface. Voids were measured by their number and size (on average void diameter was 50 μm) from macrosections. The length of cracks was measured by using an optical microscope and a X–Y position-measuring table. In total, 38 cross sections were acquired and measured.

C. Signal processing

Figure 4 shows typical OCT, plasma and back-reflection signals, and top and bottom pictures of the corresponding weld. Transitional phenomena at the beginning of the welding can be noticed from the signals (marked with a gray box in Fig. 4).

© Author(s) 2023

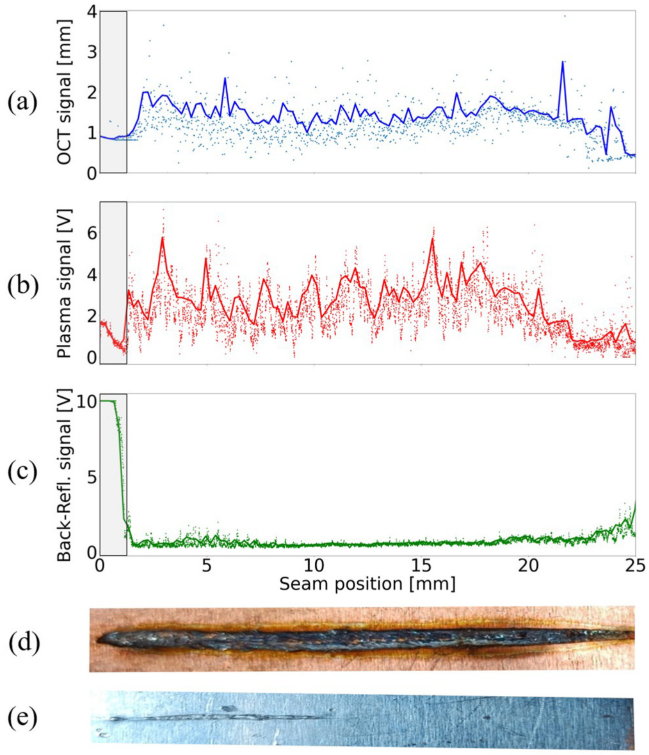

FIG. 4. Example of raw (dots) and filtered (solid line) signals: (a) OCT signal, (b) plasma signal, (c) back-reflection signal, (d) sample top view, and (e) sample bottom view.

Acquired signals were processed using the percentile filtering method, to remove high-frequency disturbances from the raw data of both photodiode and OCT signals.[18] Percentile filtering is based on a moving window (M_W) which determines the amount of data needed to be filtered in the same step, and percentile value (P_V) which determines the percentage of data lying under the filtered signal. M_W and P_V were determined with screening experiments showing $M_W = 50$ and $P_V = 80\%$ resulting in the highest accuracy, a finding also confirmed in Refs. 13 and 19. To remove the transient regime at the beginning (due to in-coupling of the laser with Cu) and end of the weld, the first and last 2.5 mm were removed from the signals.

D. Data processing

For each processing parameter in Table II, two features were extracted from each corresponding signal: (1) average signal value, U, as in Eq. (1), and (2) signal scatter, σ, as in Eq. (2),

$$U = \frac{\sum_{i=1}^{N} x(i)}{N}, \tag{1}$$

$$\sigma = \sqrt{\frac{\sum (x(i) - U)^2}{N}}, \tag{2}$$

where $x(i)$ is the value of the filtered signal at ith measured point and N is the number of measured points. Using the average and scatter values, we evaluated photodiode and OCT signals, with corresponding nomenclature U_P, U_R, U_{OCT} for signal averages and σ_P, σ_R, σ_{OCT} for signal scatters. Photodiode signals were expressed in volts (V). The OCT signal was measured in millimeters and represents the direct measurement of the keyhole depth.[14]

Measured voids and cracks within the weld cross section were further numerically evaluated. Area fraction of voids (Φ_V) was determined based on the void's relative area (A_{voids}) compared to the total weld area (A_{weld}) as in Eq. (3),

$$\Phi_V = \frac{A_{voids}}{A_{weld}}, \tag{3}$$

where A_{voids} was calculated from the number and size of voids in specific cross sections, while A_{weld} was calculated from images as the area of the entire weld.

Cracks were evaluated based on their total measured length per weld cross section (L_C).

ANOVA was used to test the null hypothesis that there is a significant difference in the signal values (plasma, back-reflection, OCT), between the different processing parameters. The significance level was set at 0.05 to ascertain the difference between the signals of the compared groups. Additionally, analysis was conducted on the correlation between the measured weld features and the obtained signals at the corresponding cross sections using Pearson's linear correlation, r. To define the strength of correlations, we used criteria as stated in Table III.

Based on the resulting strength of observed correlations, criteria to define the three weld classes were selected. A random forest classifier was adopted to evaluate the weld classification accuracy of different sensor/signal combinations. The following six cases were tested:

- plasma signal (U_P, σ_P),
- back-reflection signal (U_R, σ_R),
- OCT signal (U_{OCT}, σ_{OCT}),
- plasma and OCT (U_P, σ_P, U_{OCT}, σ_{OCT}),
- back-reflection and OCT (U_R, σ_R, U_{OCT}, σ_{OCT}), and
- fusion of all signals (U_P, σ_P, U_R, σ_R, U_{OCT}, σ_{OCT}).

TABLE III. Definition of strength for Pearson's correlation.

Absolute value of r	Strength of relationship
$r < 0.25$	No relationship
$0.25 < r < 0.5$	Weak relationship
$0.5 < r < 0.75$	Moderate relationship
$r > 0.75$	Strong relationship

© Author(s) 2023

Random forest classifier (criterion: "Gini," number of estimators: 100, max model depth: 5) is a classification algorithm made of a large number of decision trees called estimators. Results of this algorithm present classification cases and probabilities of input data corresponding to a certain class. The classifier was applied to each sensor combination in a controlled way, where a random state of the classifier's starting point and a number of estimators were fixed. Besides fixed starting parameters, the same samples were used for model fitting purposes, consisting of twelve samples, where all weld states were equally represented. This was done to evaluate differences between the analyzed cases.

III. RESULTS AND DISCUSSION

A. Variation of core power (group [1])

Figure 5 shows the signal features acquired from OCT, plasma, and back-reflection for different values of P_C. Based on average values [Figs. 5(a) and 5(b)], an upward trend between plasma and laser power and a downward trend with back-reflection can be seen (observations are all significant with a p-value below 0.05). ANOVA results for P_C variations are presented in Table IV. Throughout the whole seam length, higher plasma and lower back-reflection values were reported when welding with higher $P_{C,}$ which confirms the higher plasma radiation and better in-coupling of the laser beam while using higher laser power. In line with the average plasma and back-reflection values, scatter values also present a discernible difference between groups at 700, 1400, and 2300 W, respectively. As for the average values, a linear upward and downward trend is observed with scatter values as well.

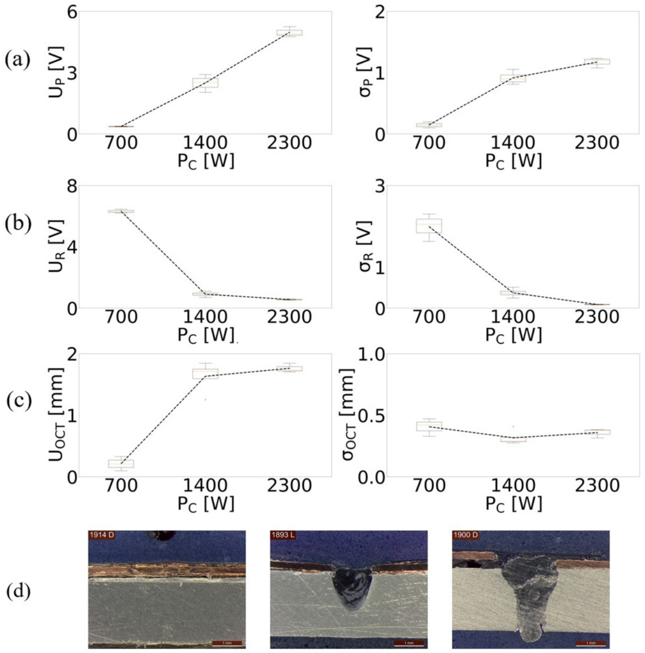

P_C = 700W (no weld) P_C = 1400W (good weld) P_C = 2300W (over weld)

FIG. 5. Boxplots of variation of core power (group [1]) with average (left) and scatter (right) values: (a) plasma signal, (b) back-reflection signal, (c) OCT signal, and (d) typical cross sections: $P_C = 700$ W (left), $P_C = 1400$ W (middle), and $P_C = 2300$ W (right).

TABLE IV. ANOVA results for P_C variations. Bold values represent statistical significance against related signals.

	P_C variations (W)		
Feature	Groups		
	700–1400	1400–2300	700–2300
U_P	$\mathbf{2 \times 10^{-4}}$	$\mathbf{1.9 \times 10^{-4}}$	$\mathbf{5.9 \times 10^{-6}}$
σ_P	$\mathbf{8.33 \times 10^{-5}}$	**0.018**	$\mathbf{5.4 \times 10^{-5}}$
U_R	$\mathbf{6 \times 10^{-8}}$	**0.018**	$\mathbf{4.0 \times 10^{-8}}$
σ_R	$\mathbf{2 \times 10^{-4}}$	**0.007**	$\mathbf{6.1 \times 10^{-4}}$
U_{OCT}	$\mathbf{3.4 \times 10^{-4}}$	0.49	$\mathbf{4.3 \times 10^{-5}}$
σ_{OCT}	0.13	0.34	0.37

This is in line with the fact that at higher power, the process tends to become more unstable due to the formation of high turbulences in the molten pool. This result is in agreement with the results presented in Ref. 6. While plasma and back-reflection show a significant difference between all three groups, the U_{OCT} signal only shows a significant difference for groups at $P_C = 700$ W and 1400 W, while there is a minor difference between 1400 and 2300 W. This can be explained by the fact that penetration depth at 1400 W is almost equal to the thickness of the Al plate. Thus, by further increasing the laser power, a through-all penetration occurs, which limits the capability of the OCT sensor.

With increasing laser power, a greater number of voids were observed in the macrosections which is consistent with the physical explanation that higher laser power increases the keyhole oscillation and molten pool dynamics, which ultimately show up as voids due to gas bubbles trapped in the molten pool.[20] Voids were mostly observed in the upper part of the weld. However, since Φ_V is normalized by the weld area, no difference was observed between the groups of different laser powers: $\Phi_V = 0.26 \pm 0.19\%$ (at $P_C = 1400$ W) and $\Phi_V = 0.22 \pm 0.12\%$ (at $P_C = 2300$ W). Cracks were observed in 80% of weld macrosections. The average length of the cracks was 1.0 ± 0.7 mm. No discernable differences regarding the average length of cracks were observed for different P_C values, except for a group of 700 W, where no cracking and voids were observed since no weld was achieved [see Fig. 5(d)].

B. Variation of focal offset (group [2])

Figure 6 reports statistical features of signals acquired for OCT and photodiodes for different values of A_Z.

No significant difference was observed between any of the A_Z groups for average plasma, back-reflection, and OCT signals. Based on macrosection inspection, this is in line with the achieved laser process, as typical welds [see Fig. 6(d)] presented no discernable difference in weld depth and interface width for $A_Z = 5$, 7, 10 mm groups. While deeper welds were observed in group $A_Z = 3$ mm, the difference was not clearly captured by the OCT sensor. These observations are in line with system characteristic and show that

© Author(s) 2023

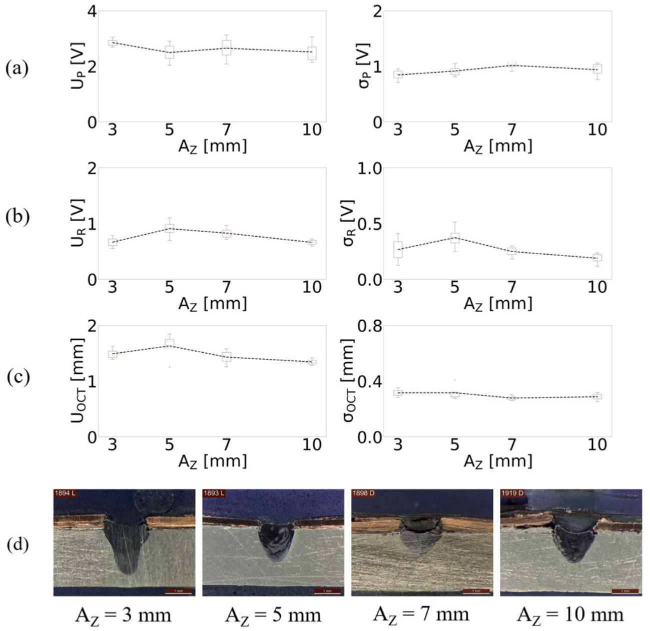

FIG. 6. Boxplots of variation of focal offset (group [2]) with average (left) and scatter (right) values: (a) plasma signal, (b) back-reflection signal, (c) OCT signal, and (d) typical cross sections: $A_Z = 3, 5, 7, 10$ mm (from left to right).

focal offsets larger than Rayleigh's length (2.6 mm) have small effect on the laser process of the chosen application. No difference between scatter values was observed. In line with Fig. 5(c), OCT scatter values around 0.4 mm were observed, which shows that the OCT sensor is not affected by different laser process parameters.

Based on the obtained ANOVA results (see Table V), A_Z variations present no effect on the laser welding process for the selected application, while a trend of a decreasing signal for plasma and OCT value was observed for groups $A_Z = 7$ and 10 mm. This can be contributed to decreased laser intensities with higher defocus offsets, compared to the Rayleigh's length of the laser system.

With the increase of focal offset, no changes were observed in terms of area fraction of voids ($\Phi_v = 0.20 \pm 0.18\%$), except for the group $A_Z = 10$ mm, where a big rise was seen ($\Phi_v = 0.74 \pm 0.61\%$). The fact that this presents a big offset compared to the Rayleigh length (2.6 and 6.2 mm for core and ring beam) of the laser source is a major cause for this result as more unstable welding conditions were expected. No difference in terms of the average length of the cracks ($L_C = 0.85 \pm 0.63$ mm) was observed.

TABLE V. ANOVA results for A_Z variations.

	A_Z variations (mm)			
Feature	Groups			
	3–5	5–7	3–7	7–10
U_P	0.19	0.66	0.57	0.76
σ_P	0.45	0.24	0.13	0.51
U_R	0.09	0.52	0.18	0.11
σ_R	0.31	0.14	0.85	0.30
U_{OCT}	0.43	0.29	0.63	0.45
σ_{OCT}	0.99	0.36	0.19	0.70

C. Correlations between signals and cross sections

Correlations between statistical features and weld features: weld depth (d_M), weld width (w_M), area fraction of voids (Φ_V), and crack length (L_C) have been evaluated. Figure 7 visually presents Pearson's correlations between the average values of plasma, back-reflection, and OCT in relation to the d_M and w_M. Figure 8 shows the full correlation matrix.

Results show a strong correlation ($r = 0.77$) between the OCT signal and the actual penetration depth, which implies that the processed depth from the OCT sensor can be used for measuring and controlling the weld depth during the welding process. With a strong correlation between weld depth and weld interface width ($r = 0.87$), we can presume a conical shape of the welds, which was also observed during cross section analysis [Fig. 5(d), $P_C = 1400$ W].

Correlation value between d_M and U_P ($r = 0.87$) further demonstrates a very strong relation between plasma signal and the achieved depth, which was also observed in Fig. 5(a). This result agrees with the fact that a higher plasma plume occurs at higher laser power, and deeper welds are achieved.

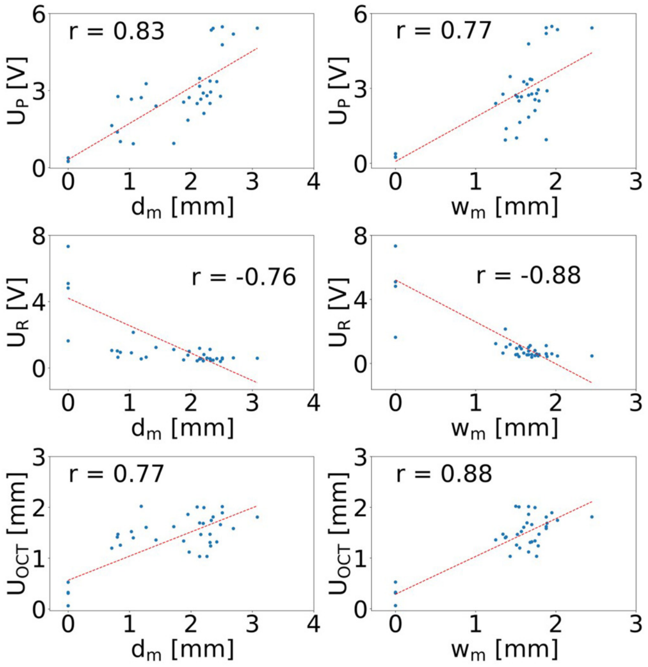

FIG. 7. Correlation graphs between measured weld dimensions (d_M and w_M) and signals for photodiodes and OCT.

© Author(s) 2023

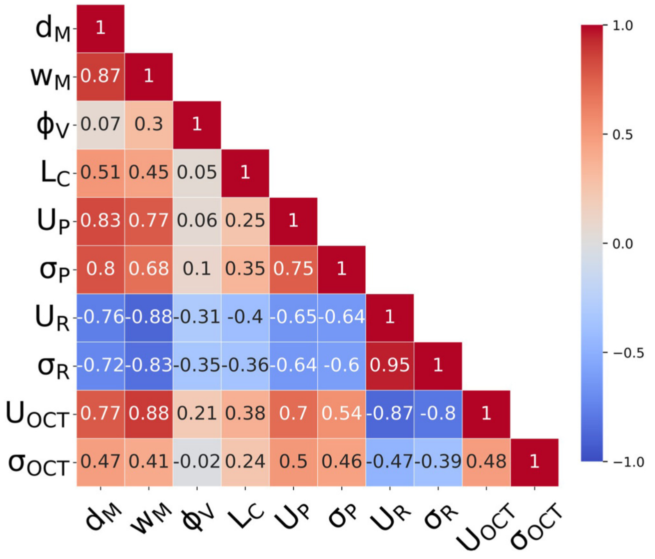

	d_M	w_M	ϕ_V	L_C	U_P	σ_P	U_R	σ_R	U_{OCT}	σ_{OCT}
d_M	1									
w_M	0.87	1								
ϕ_V	0.07	0.3	1							
L_C	0.51	0.45	0.05	1						
U_P	0.83	0.77	0.06	0.25	1					
σ_P	0.8	0.68	0.1	0.35	0.75	1				
U_R	-0.76	-0.88	-0.31	-0.4	-0.65	-0.64	1			
σ_R	-0.72	-0.83	-0.35	-0.36	-0.64	-0.6	0.95	1		
U_{OCT}	0.77	0.88	0.21	0.38	0.7	0.54	-0.87	-0.8	1	
σ_{OCT}	0.47	0.41	-0.02	0.24	0.5	0.46	-0.47	-0.39	0.48	1

FIG. 8. Correlation matrix between weld features (d_M, w_M, Φ_V, and L_C) and signals features.

A negative strong correlation between back-reflection U_R and w_M ($r = -0.88$) is acknowledged from the data, which can also be compared with the observations of U_R from Fig. 5(b). This translates to the fact that a higher back-reflection occurs in case of poor beam in-coupling (and partial or incomplete fusion of the material being processed).

A strong correlation ($r = 0.88$) between U_{OCT} and w_M is also presented, which is in line with the combined effect of $w_M - d_M$ and $U_{OCT} - d_M$. This comes from the fact that a wider measured weld width was seen with deeper welds and a good traceability of penetration depth was seen by its correlation to U_{OCT} signal; this further provides us with the evidence that OCT is beneficial for tracking the penetration depth when a keyhole is established.

Based on the observed correlations, criterion for the definition of weld classes was selected. In literature, many different criteria for defining the quality of the weld are defined. From basic, where only one weld feature is observed (e.g., weld depth and weld width on the bottom side), to more advanced, where different visual and mechanical characteristics (e.g., underfill, undercut, tensile strength, and electrical resistivity) are observed and measured. In case of thin sheet metals, Du *et al.*[17] investigated the optimum weld depth for maximum weld strength by developing a geometrical model and conducting tensile-shear tests on lap-welded steel sheets of 100 μm thickness. The study concludes that the weld depth should be around 1.5 times the thickness of the upper sheet for sufficient weld strength. For our investigation, basic weld features were selected to be the main objective of inspection. Three weld classes have been defined, driven by the need to control the weld depth,

- "No weld" occurs when $d_M = 0$.
- "Good weld" occurs when $0 < d_M < t$.
- "Over weld" occurs when $d_M \geq t$.

TABLE VI. Results of the classification using the Random Forest algorithm.

Signal fusion combinations	Classification accuracy (%)
U_P and σ_P	84.21
U_R and σ_R	78.95
U_{OCT} and σ_{OCT}	71.05
U_P, σ_P, U_{OCT}, σ_{OCT}	86.84
U_R, σ_R, U_{OCT}, σ_{OCT}	78.95
U_P, σ_P, U_R, σ_R, U_{OCT}, σ_{OCT}	84.21

Due to the strong correlation between d_M and w_M, the interface width was not included in defining weld classes. Since only weak correlations between Φ_V, L_C, and sensor signals were observed, these features were also not included in the weld class definition.

D. Classification of weld classes

Random forest classification results are listed in Table VI and Fig. 9, where classification accuracy is expressed in percentage and represents the ratio between the number of correct predictions and the total number of tested cases. Low accuracy corresponds to a high level of misclassification. From the results of different signal combinations, we can see that the classification based only on plasma is as accurate as the fusion of all acquired signals (plasma, back-reflection, and OCT). Classification is based only on back-reflection and OCT results in low classification accuracy with a majority of the misclassification cases being detected between "good weld" and "over weld."

This misclassification behavior was expected based on the already acquired knowledge from Figs. 5(b) and 5(c). A significant difference was observed in U_R and U_{OCT} signals between certain laser parameter groups, which were later classified as "no weld" and "good weld"/"over weld." However, little signal value differences were observed between laser parameter groups that later corresponded to "good" and "over weld" groups. Furthermore, the fusion of back-reflection and OCT signals did not present an improvement in classification accuracy and reduced misclassification cases. However, the fusion of plasma and OCT presented the best results in classification accuracy, with one less misclassified case compared to plasma only and the fusion of all three sensors. The addition of OCT signal to plasma corrected three cases of classified "good welds"-s as "over weld"-s by exhibiting a low U_{OCT} signal. The fusion effect also resulted in two misclassified "over weld" specimens as "good weld" and not contributing to any classification change to three wrongly predicted cases during the plasma-only classification.

Complementing results were observed (see Table VII) for different weld classes in terms of weld features as well. More voids and longer cracks were observed for the "over weld" class compared to the "good weld" class. This is in line with the results of P_C and A_Z variations where too much power, or a bigger focal offset, resulted in more voids and cracks. For the "over weld" class through-weld cracks, root-weld cracks and occurrence of bigger voids were observed, while minor cracks and no big voids were observed in "good weld" cases.

© Author(s) 2023

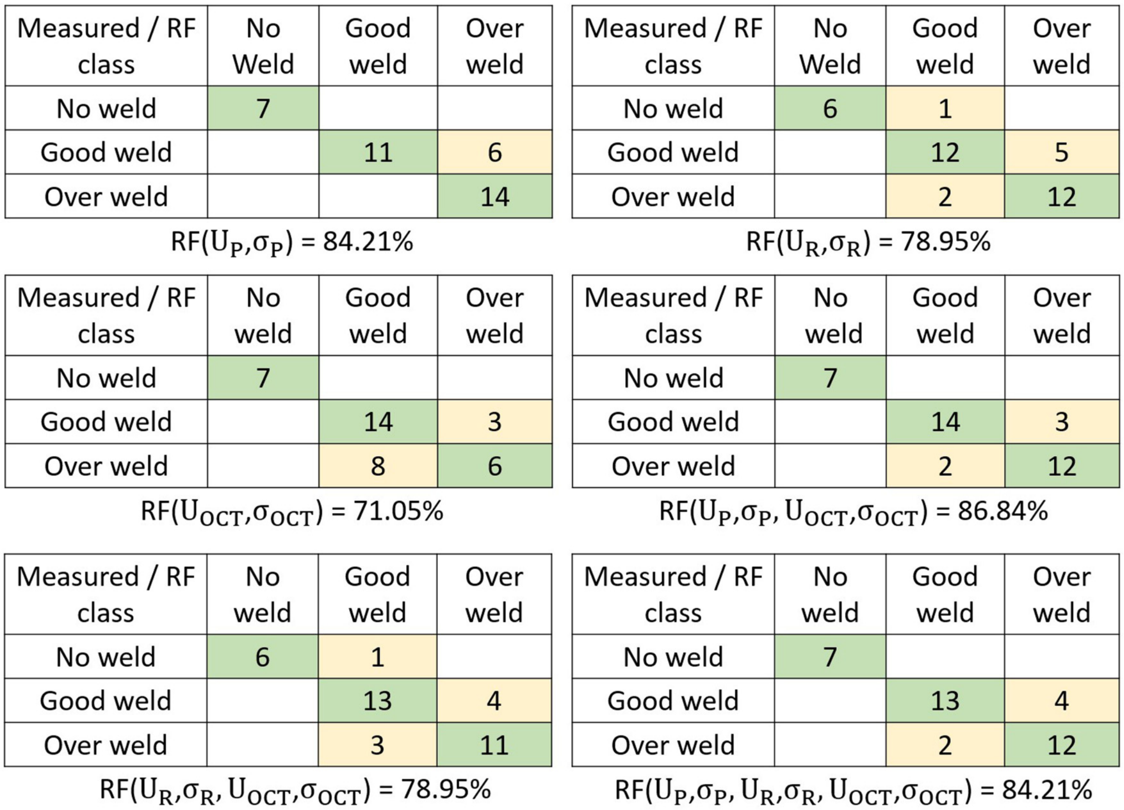

Measured / RF class	No Weld	Good weld	Over weld
No weld	7		
Good weld		11	6
Over weld			14

RF(U_P,σ_P) = 84.21%

Measured / RF class	No Weld	Good weld	Over weld
No weld	6	1	
Good weld		12	5
Over weld		2	12

RF(U_R,σ_R) = 78.95%

Measured / RF class	No weld	Good weld	Over weld
No weld	7		
Good weld		14	3
Over weld		8	6

RF(U_{OCT},σ_{OCT}) = 71.05%

Measured / RF class	No weld	Good weld	Over weld
No weld	7		
Good weld		14	3
Over weld		2	12

RF(U_P,σ_P, U_{OCT},σ_{OCT}) = 86.84%

Measured / RF class	No weld	Good weld	Over weld
No weld	6	1	
Good weld		13	4
Over weld		3	11

RF(U_R,σ_R, U_{OCT},σ_{OCT}) = 78.95%

Measured / RF class	No weld	Good weld	Over weld
No weld	7		
Good weld		13	4
Over weld		2	12

RF(U_P,σ_P, U_R,σ_R, U_{OCT},σ_{OCT}) = 84.21%

FIG. 9. Confusion matrices for all the signal combinations ("RF class" corresponds to the prediction of the random forest classifier).

While a certain level of classification can be achieved by only using plasma signal, there are advantages of fusion with the OCT signal in terms of acquiring a direct measurement of weld penetration depth. Thus, the scalability of the monitoring system can be much wider by also using the OCT. However, different noise sources exert influence on the values of the OCT sensor during laser welding. Figures 5(c) and 6(c) show an OCT scatter value of around 0.4 mm, which is twice as much as the thickness of the Cu thin plate. Although the alignment of the OCT beam was pre-optimized in preliminary screening sessions, the OCT accuracy could be affected by using a wobbling technique, where positioning of the OCT beam inside the bottom part of the keyhole due to the laser beam and keyhole movement on the material surface proved challenging. Wrong alignment of the OCT beam can imply changes to the scatter, which was reported by Sokolov *et al.*[13] Additionally, chromatic aberrations of the OCT beam were reported in using OCT for medical applications.[21]

TABLE VII. Results of weld features for weld classes.

Weld feature	No weld	Good weld	Over weld
d_M (mm)	0	1.48 ± 0.55	2.43 ± 0.23
w_M (mm)	0	1.54 ± 0.16	1.85 ± 0.20
Φ_V (%)	0	0.38 ± 0.14	0.25 ± 0.18
L_C (mm)	0	0.85 ± 0.79	0.98 ± 0.65

Although a higher welding speed provided a wider process window, it could have affected the accuracy of acquired signals as well. With increased welding speed, the occurrence of a more inclined keyhole is reported by Fabbro *et al.*[22] This could present us with a lower OCT depth signal than the actual weld depth, since bottom of the keyhole is no longer aligned with the laser beam incidence angle. This shows that future improvement of the OCT technology is necessary and has a big potential to increase the accuracy of process monitoring and control. For example, better precision could be achieved by using galvo scanner optics for OCT beam guidance,[23] while advances in OCT signal processing are still needed.

IV. CONCLUSIONS AND FINAL REMARKS

This paper investigated the fusion of OCT and photodiode sensors for the diagnosis of weld features during RLW of Cu-to-Al welding. The main interest was to present the unique benefits and competitive advantages of both sensors in the case of two manufacturing scenarios: variation of laser power and variation of focal offset. In further studies, the effect of other laser welding parameters (e.g., welding speed, oscillation frequency, and amplitude) can be examined further.

Main findings: (1) Plasma is the predominant signal, which carries most of the information about the process and is well correlated to the variations of the laser power. (2) Variations of the focal offset are well represented by back reflection and predominantly by the scatter level. However, misclassifications between "no weld" and "good weld" have been observed. (3) Strong correlation ($r > 0.75$) between sensors (plasma, back-reflection, and OCT) and weld dimensions is encouraging for the deployment of inprocess monitoring solutions.

Analysis of misclassifications: (1) The information carried out by the OCT sensor does not enable unique distinction between "good weld" and "over weld" with significant variation of the weld penetration depth. The same conclusion applies to the plasma signal as well. (2) Owing to the fact that the process window is significantly small when welding thin foils (below 500 μm) and the interaction between parameters generate process instability (i.e., high reflections due to the nature of copper), variations in the process are eventually not captured by the signal features, resulting in increased confusion during classification. This is particularly evident in the misclassifications between "no weld" and "good weld."

Sensor fusion: (1) OCT sensor allowed detecting "no weld" scenarios, while the variations between "good weld" and "over weld" were barely detected. (2) Photodiodes could detect differences for all three classes ("no weld," "good weld," and "over weld"). However, the photodiode results are only valid under the tested conditions of P_C and A_Z variations; for instance, adding inert gas or changes to the material alloys would result in different signal values due to plasma intensities and reflectivity variations at the same achieved penetration depths. (3) With the addition of multiple weld features (weld interface width, top seam width, concavity, porosity, etc.), a sensor fusion strategy with multiple sensors (e.g., OCT, photodiodes, and laser scanners) would allow reducing misclassifications. (4) However, investment and maintenance costs must be considered. Low-cost photodiodes can be exploited for use in high-volume manufacturing, while the fusion of multiple sensors would be particularly useful in low-volume production, where processing parameters and materials/geometries are frequently changed (mass customization with high product variety).

ACKNOWLEDGMENTS

This study was financially supported by (1) WMG HVM Catapult, (2) APC UK project: ALIVE—Aluminium Intensive Vehicle Enclosures, (3) Innovate UK FASA: Flexible, Automated Stator Assembly, (4) Slovenian Research Agency (research core funding No. P2-0392). We acknowledge the contribution and support of the Student Exchange Program between The University of Warwick and University of Ljubljana.

NOMENCLATURE

A_Z = focal offset (mm)
A_Y = lateral oscillation amplitude (mm)
d_M = measured weld depth (mm)
f = oscillation frequency (Hz)
L_C = measured crack length (mm)
P_C = laser core power (W)
P_R = laser ring power (W)
r = Pearson's correlation coefficient
S_X = welding velocity (mm/s)
U_P = average value of plasma (V)
U_R = average value of back-reflection (V)
U_{OCT} = OCT average depth value (mm)
w_M = measured weld width (mm)
σ_P, σ_R = signal standard deviation (V)
σ_{OCT} = OCT signal standard deviation (mm)
Φ_V = area fraction of voids (%)

AUTHOR DECLARATIONS

Conflict of Interest

The authors have no conflicts to disclose.

Author Contributions

Tine Brežan: Conceptualization (equal); Data curation (equal); Formal analysis (equal); Investigation (equal); Methodology (equal); Validation (equal); Visualization (lead); Writing – original draft (lead). **Pasquale Franciosa:** Conceptualization (equal); Data curation (equal); Formal analysis (equal); Funding acquisition (equal); Investigation (equal); Methodology (equal); Resources (equal); Supervision (equal); Writing – review & editing (equal). **Matija Jezeršek:** Conceptualization (equal); Data curation (supporting); Formal analysis (equal); Funding acquisition (equal); Resources (equal); Supervision (equal); Writing – review & editing (equal). **Dariusz Ceglarek:** Conceptualization (equal); Data curation (supporting); Formal analysis (supporting); Funding acquisition (equal); Resources (equal); Supervision (equal); Writing – review & editing (equal).

REFERENCES

[1] M. Kos, E. Arko, H. Kosler, and M. Jezeršek, "Remote laser welding with in-line adaptive 3D seam tracking," Int. J. Adv. Manuf. Technol. **103**, 4577–4586 (2019).

[2] A. Fortunato and A. Ascari, "Laser welding of thin copper and aluminum sheets: Feasibility and challenges in continuous-wave welding of dissimilar metals," Lasers Manuf. Mater. Process. **6**, 136–157 (2019).

[3] M. Kos, E. Arko, H. Kosler, and M. Jezeršek, "Penetration-depth control in a remote laser-welding system based on an optical triangulation loop," Opt. Lasers Eng. **139**, 106464 (2021).

[4] A. Božič, M. Kos, and M. Jezeršek, "Power control during remote laser welding using a convolutional neural network," Sensors **20**, 6658 (2020).

[5] D. Y. You, X. D. Gao, and S. Katayama, "Review of laser welding monitoring," Sci. Technol. Weld. Join. **19**, 181–201 (2014).

[6] G. Chianese, P. Franciosa, J. Nolte, D. Ceglarek, and S. Patalano, "Characterization of photodiodes for detection of variations in part-to-part gap and weld penetration depth during remote laser welding of copper-to-steel battery Tab connectors," J. Manuf. Sci. Eng. **144**, 071004 (2022).

[7] J. Stavridis, A. Papacharalampopoulos, and P. Stavropoulos, "Quality assessment in laser welding: A critical review," Int. J. Adv. Manuf. Technol. **94**, 1825–1847 (2018).

© Author(s) 2023

[8] P. Franciosa, M. Sokolov, T. Sun, G. Chianese, and D. Ceglarek, "Laser welding: High volume manufacturing for E-mobility," Laser User Mag. Spons. AILU **99**, 24–25 (2021).
[9] N. D. Dupriez and A. Denkl, "Advances of OCT technology for laser beam processing: Precision and quality during laser welding," Laser Tech. J. **14**, 34–38 (2017).
[10] Z. Jiang, Z. Jiang, and H. Ding, "Optical coherence tomography for laser welding applications," Optik **257**, 168784 (2022).
[11] C. Stadter, M. Schmoeller, L. von Rhein, and M. F. Zaeh, "Real-time prediction of quality characteristics in laser beam welding using optical coherence tomography and machine learning," J. Laser Appl. **32**, 022046 (2020).
[12] M. Schmoeller, C. Stadter, S. Liebl, and M. F. Zaeh, "Inline weld depth measurement for high brilliance laser beam sources using optical coherence tomography," J. Laser Appl. **31**, 022409 (2019).
[13] M. Sokolov, P. Franciosa, R. Al Botros, and D. Ceglarek, "Keyhole mapping to enable closed-loop weld penetration depth control for remote laser welding of aluminum components using optical coherence tomography," J. Laser Appl. **32**, 032004 (2020).
[14] M. Sokolov *et al.*, "Applying optical coherence tomography for weld depth monitoring in remote laser welding of automotive battery tab connectors," J. Laser Appl. **33**, 012028 (2021).
[15] V. Dimatteo, A. Ascari, and A. Fortunato, "Continuous laser welding with spatial beam oscillation of dissimilar thin sheet materials (Al-Cu and Cu-Al): Process optimization and characterization," J. Manuf. Process. **44**, 158–165 (2019).
[16] M. Miyagi and X. Zhang, "Investigation of laser welding phenomena of pure copper by x-ray observation system," J. Laser Appl. **27**, 042005 (2015).
[17] J. Du, J. Longobardi, W. P. Latham, and A. Kar, "Weld strength and process controllability for laser welding of thin sheet metals," J. Laser Appl. **12**, 239 (2000).
[18] M. Boley, F. Fetzer, R. Weber, and T. Graf, "Statistical evaluation method to determine the laser welding depth by optical coherence tomography," Opt. Lasers Eng. **119**, 56–64 (2019).
[19] C. Mittelstädt, T. Mattulat, T. Seefeld, and M. Kogel-Hollacher, "Novel approach for weld depth determination using optical coherence tomography measurement in laser deep penetration welding of aluminum and steel," J. Laser Appl. **31**, 022007 (2019).
[20] F. Lu, X. Li, Z. Li, X. Tang, and H. Cui, "Formation and influence mechanism of keyhole-induced porosity in deep-penetration laser welding based on 3D transient modeling," Int. J. Heat Mass Transf. **90**, 1143–1152 (2015).
[21] W. Drexler, Y. Chen, A. Aguirre, B. Povăzay, A. Unterhuber, and J. G. Fujimoto, "Ultrahigh resolution optical coherence tomography," in *Optical Coherence Tomography: Technology and Applications*, edited by W. Drexler and J. G. Fujimoto (Springer, Berlin, 2008), pp. 239–279.
[22] R. Fabbro and K. Chouf, "Dynamical description of the keyhole in deep penetration laser welding," J. Laser Appl. **12**, 142–148 (2000).
[23] V.-F. Duma, P. Tankam, J. Huang, J. Won, and J. P. Rolland, "Optimization of galvanometer scanning for optical coherence tomography," Appl. Opt. **54**, 5495 (2015).

© Author(s) 2023